



**SIMULATION OF GROUND MOTIONS DURING
THE 1993 HOKKAIDO-NANSEI-OKI EARTHQUAKE
BY EMPIRICAL GREEN'S FUNCTION METHOD
AND STOCHASTIC GREEN'S FUNCTION METHOD
– VERIFICATION OF CHARACTERIZING PROCEDURE OF
EARTHQUAKE SOURCE MODEL FOR STRONG MOTION
PREDICTION –**

Akira FUKUKITA¹, Jun'ichi MIYAKOSHI², Kazuo DAN³, and Kazuhiko YASIRO⁴,

SUMMARY

We simulated strong ground motions during the 1993 Hokkaido-Nansei-Oki, Japan, earthquake (M_{JMA} 7.8) based on its variable-slip rupture model and on its characterized asperity models to verify the characterizing procedure of source models by Dan *et al.* [1] for the strong motion prediction in future earthquakes. The asperity models were characterized by the total seismic moment, the short-period level of the source spectra, and the ratios of the area, the final slip, and the effective stress on the asperity to those on the entire fault.

First, the empirical Green's function method was applied to the simulation of the records at JMA Sapporo, about 170 km far from the fault. Next, the stochastic Green's function method was applied to the wide area (192,000 km²) including the epicentral region.

From the results, the characterized asperity model was useful for the simulation of the strong motion prediction in the wide area including the epicentral region.

INTRODUCTION

It is very important to predict the strong ground motions in future earthquakes for considering the measure to reduce earthquake disaster, and the information of the prediction is basic data. It is necessary to take into account of the complexity of the fault rupture for predicting the strong motions with sufficient accuracy, and two methods are adopted for this. The one is to use variable-slip rupture models for past earthquakes which is proposed by Heaton *et al.* [2], and the other is to use characterized models based on

¹ Research engineer, Shimizu Corporation, Tokyo, Japan. Email: fukukita@shimz.co.jp

² Deputy senior research engineer, Shimizu Corporation, Tokyo, Japan. Email: miyakoshi@shimz.co.jp

³ Senior research engineer, Shimizu Corporation, Tokyo, Japan. Email: kazuo.dan@shimz.co.jp

⁴ Tokyo Electric Power Company, Japan. Email: yasiro.k@tepcoco.jp

the fractal model proposed by Kikuchi and Fukao [3], the wave-number spectrum model by Somerville *et al.* [4], or the asperity model proposed by Somerville *et al.* [4].

The asperity model proposed by Somerville *et al.* [4] consists of the asperity and the background. The final slip is relatively large on the asperity, and it is relatively small on the background.

Among the parameters (position, strike, dip, rake, area, final slip, effective stress, hypocenter, rupture velocity, rupture mode, and so on) concerned with the asperity and the background of the asperity model, Irikura and Miyake [5] evaluated the area and the final slip by the results of Somerville *et al.* [4] for long-period earthquake motions, and evaluated the effective stress by the static stress drop for a circular crack of Eshelby [6]. The characterizing procedure of the source by Irikura and Miyake [5] was verified for the inland earthquakes of magnitude 7 such as the 1994 Northridge earthquake [7] and the 1995 Hyogo-ken Nanbu earthquake [8].

Dan *et al.* [1] proposed a new characterizing procedure of the source which evaluated the effective stress on the asperity and the background considering the level of the acceleration source spectrum in the short-period range, called short-period level by Dan and Sato [9]. This method was intended for inland and subduction earthquakes.

The object of this study is to verify the characterizing procedure of the source for the strong motion prediction in future earthquakes. Here, we simulated strong ground motions during the 1993 Hokkaido-Nansei-Oki, Japan, earthquake (M_{JMA} 7.8) because the detail source inversion models, records, and distribution of the seismic intensity have been obtained for this earthquake. We used variable-slip rupture model and two types of characterized asperity models.

First, the empirical Green's function method was applied to the actual calculation of the records at JMA Sapporo about 170 km far from the fault.

Next, the stochastic Green's function method was applied to every 1 km² in the wide area including the epicentral region.

SOURCE MODEL OF THE 1993 HOKKAIDO-NANSEI-OKI EARTHQUAKE

Variable-slip rupture model

There are several source models for the 1993 Hokkaido-Nansei-Oki earthquake obtained by source inversions (e.g. Kikuchi *et al.* [10], Imanishi *et al.* [11], Takehi and Irikura [12], Mendoza and Fukuyama [13]). In this study, we used a variable-slip rupture model inverted by Mendoza and Fukuyama [13], which had used the teleseismic data and the displacement data of strong motions. Figure 1 shows the northeastern part of Japan including southern Hokkaido and northern Tohoku, where we simulated the strong ground motions. It also shows the fault model of the mainshock, and the locations of JMA Sapporo and JMA Akita. This figure includes the epicenter of the mainshock determined by the JMA (star) and by Harvard University (square) [14], and the epicenters of the aftershocks (triangles) with the focal mechanisms. Figure 2 shows the distribution of seismic moment, final slip, effective stress, and short-period level derived from the variable-rupture model by Mendoza and Fukuyama [13]. Mendoza and Fukuyama [13] used the records with longer period components than 2 seconds and with the predominant period of 10 seconds. The distribution of the seismic moment and the final slip shown in Figures 2a and 2b are taken from Mendoza and Fukuyama [13], and the distribution of the effective stress and the short-period level are

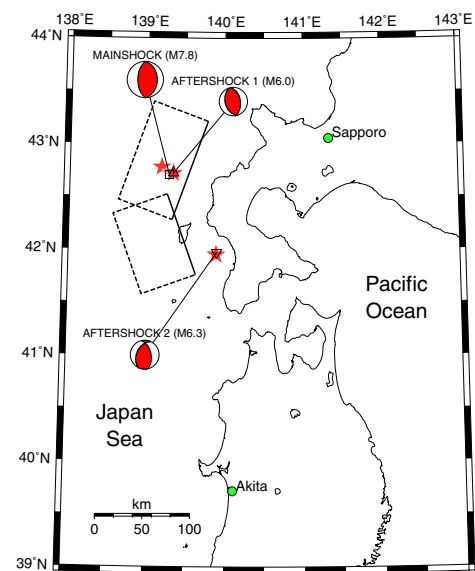


Figure 1 Study area

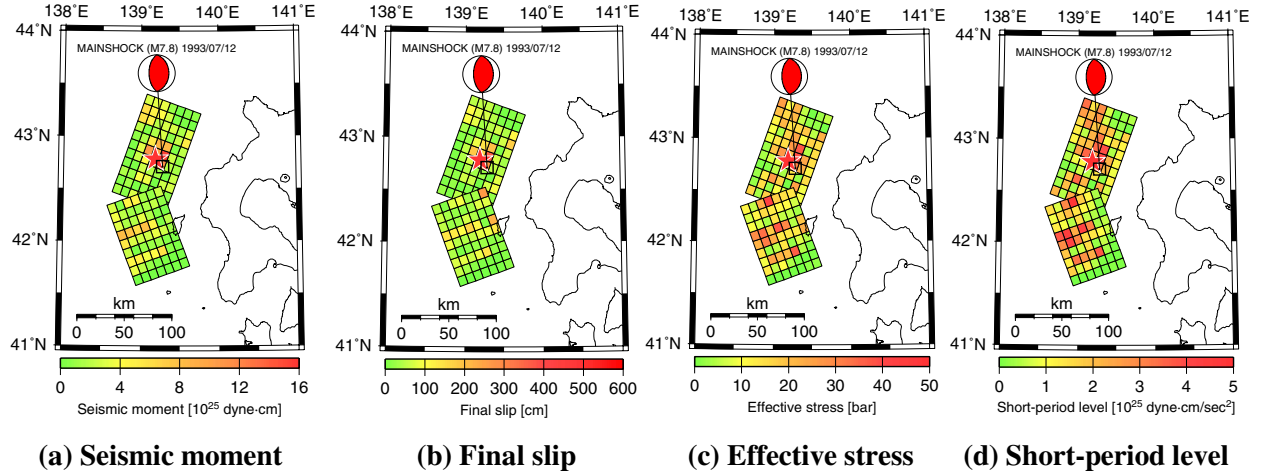


Figure 2 Variable-slip rupture model of 1993 Hokkaido-Nansei-Oki earthquake inverted by Mendoza and Fukuyama [13]

calculated by the equations (1) and (2) with the slip velocity time function inverted by Mendoza and Fukuyama [13],

$$\sigma_{pq} = \rho_{pq} \beta_{pq} V_{pq} / 2 , \quad (1)$$

$$A_{pq} = 4\pi \lambda_{pq} \sigma_{pq} \beta_{pq}^2 , \quad (2)$$

where σ is the effective stress, A is the short-period level, the subscript pq means the (p,q) th subfault, ρ is the density of the medium, β is the S-wave velocity of the medium, V is the velocity averaged over the time when slip time function grows from 10% to 70% of the final slip, and λ is the equivalent radius of the fault ([1], [9]).

Table 1 lists properties of the medium at the source, and Table 2 summarizes the source parameters of the 1993 Hokkaido-Nansei-Oki earthquake.

Characterized asperity model

The characterized asperity models are obtained from the variable-slip rupture model by the method of Dan *et al.* [1]. The seismic moment and the short-period level of the north fault and the south fault are the same as those of the variable-slip rupture model for the respective fault. Two asperity models are used in this study. The one is “model A”, whose asperity is arranged at the shallow position according to the final slip distribution of the variable-slip rupture model. The other is “model B”, whose asperity is arranged at the deep position according to the short-period level distribution of the variable-slip rupture model.

The seismic moment M_0 and the short-period level A are described by

$$M_0 = M_{0asp} + M_{0back} , \quad (3)$$

$$A^2 = A_{asp}^2 + A_{back}^2 , \quad (4)$$

where subscript *asp* is for the asperity and *back* is for the background. When we write the ratio of the area, the final slip, and the effective stress on the asperity to those on the entire fault by

$$\gamma_S = S_{asp} / S, \quad \gamma_D = D_{asp} / D, \quad \gamma_\sigma = \sigma_{asp} / \sigma , \quad (5)$$

the seismic moment and the short-period level of the asperity models are obtained as follows:

$$M_{0asp} = \gamma_S \gamma_D M_0 , \quad (6)$$

$$M_{0back} = M_0 - M_{0asp} , \quad (7)$$

Table 1 Properties of the medium at the source

Layer No.	North fault			South fault		
	Depth (km)	Density (g/cm ³)	S-wave velocity (km/s)	Depth (km)	Density (g/cm ³)	S-wave velocity (km/s)
$q = 1$	5 – 10	2.7	3.3	2 – 7	2.3	2.0
2	10 – 15	2.8	3.6	7 – 12	2.7	3.3
3	15 – 20	2.9	3.8	12 – 17	2.9	3.8
4	20 – 25	3.2	4.3	17 – 22	3.0	4.0
5	25 – 30	3.2	4.3	22 – 27	3.2	4.3
6	30 – 35	3.2	4.3	27 – 32	3.2	4.3
7	35 – 40	3.2	4.3	32 – 37	3.2	4.3

Table 2 The source parameters of the 1993 Hokkaido-Nansei-Oki earthquake

Date		12 July 1993	
Epicenter		42° 46' 48" N, 139° 11' 00" E	
Focal depth	(km)	35.1	
Magnitude	M_{JMA}	7.8	
Seismic moment	(dyne-cm)	3.4×10^{27}	
Short-period level	(dyne-cm/s ²)	2.14×10^{26}	
Strike [14]		N179E	
Dip [14]		55W	
Rake [14]		90	

Seismic moment [13]	(dyne-cm)	North fault 2.04×10^{27}	South fault 1.36×10^{27}
Short-period level	(dyne-cm/s ²)	1.56×10^{26}	1.46×10^{26}
Strike [13]		N200E	N160E
Dip [13]		30W	30W
Rake [13]		90	90
Fault length [13]	(km)	110	90
Fault width [13]	(km)	70	70

$$A_{asp} = \sqrt{(1 - \gamma_s) \gamma_s \gamma_\sigma^2 / \{ (1 - \gamma_s) \gamma_s \gamma_\sigma^2 + (1 - \gamma_s \gamma_\sigma)^2 \}} A , \quad (8)$$

$$A_{back} = \sqrt{A^2 - A_{asp}^2} , \quad (9)$$

Here, μ is the rigidity of the medium at the source, and β is the average S-wave velocity of the medium at the source, and the following equations are used:

$$M_0 = \mu S D , \quad (10)$$

$$M_{0asp} = \mu S_{asp} D_{asp} , \quad (11)$$

$$S = S_{asp} + S_{back} , \quad (12)$$

$$A_{asp} = 4\pi \sqrt{S_{asp} / \pi} \sigma_{asp} \beta^2 , \quad (13)$$

$$A_{back} = 4\pi \sqrt{S_{back} / \pi} \sigma_{back} \beta^2 , \quad (14)$$

$$\sigma = (\sigma_{asp} S_{asp} + \sigma_{back} S_{back}) / S . \quad (15)$$

Next, when we write the number of the subfaults of the entire fault as $a \times b$ and the number of the subfaults of the asperity as $a^\# \times b^\#$, we obtain the seismic moment and the effective stress of the asperity by

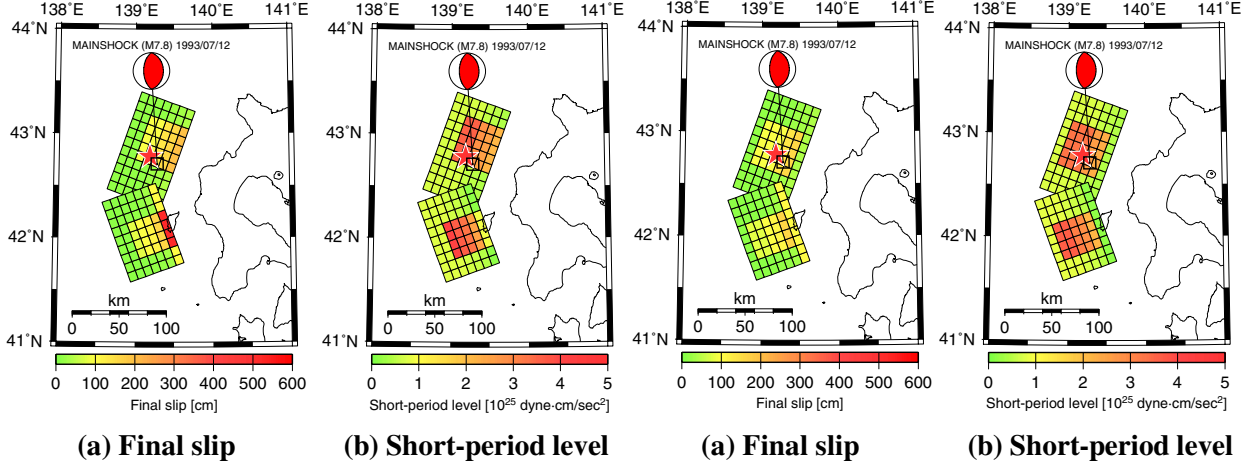


Figure 3 Characterized asperity model A, whose asperity is arranged at the shallow position according to the final slip distribution of the variable-slip rupture model

Figure 4 Characterized asperity model B, whose asperity is arranged at the deep position according to the short-period level distribution of the variable-slip rupture model

$$M_{0pq} = M_{0asp} / (a^{\#} b^{\#}) , \quad (16)$$

$$\sigma_{pq} = A_{asp} \sqrt{\pi / S_{pq}} / (4\pi \sqrt{\sum_{asp} \beta^4_{pq}}) , \quad (17)$$

and we obtain the seismic moment and the effective stress of the background by

$$M_{0pq} = M_{0back} / (ab - a^{\#} b^{\#}) , \quad (18)$$

$$\sigma_{pq} = A_{back} \sqrt{\pi / S_{pq}} / (4\pi \sqrt{\sum_{back} \beta^4_{pq}}) , \quad (19)$$

where \sum_{asp} and \sum_{back} are the summation for the subfault of the asperity and the subfault of the background, respectively. We calculate the final slip and the short-period level as follows:

$$D_{pq} = M_{0pq} / (\mu_{pq} S_{pq}) , \quad (20)$$

$$A_{pq} = 4\pi \sqrt{S_{pq}} / \pi \sigma_{pq} \beta^2_{pq} . \quad (21)$$

Here, we assumed the ratio of the area, the final slip, and the effective stress on the asperity to those on the entire fault as $\gamma_s = 0.35$, $\gamma_D = 2$, $\gamma_\sigma = 2$, referring to Ishii *et al.* [15].

We modeled the asperity as square or close to square based on the characterized asperity model by Somerville *et al.* [4], and the number of the subfault is 5 x 5 in the north fault, and 4 x 5 in the south fault. The size of the subfault is 10 km x 10 km which is equal to the model of Mendoza and Fukuyama [13].

Figures 3 and 4 show the distribution of the final slip and the short-period level of the characterized asperity models A and B, respectively. They show that the final slip becomes larger as the subfault shallower, because the rigidity varies with the depth. On the other hand, the short-period level becomes smaller as the subfault becomes shallower. Table 3 lists the seismic moment and the effective stress of the asperity and the background.

Table 3 Seismic moment and effective stress of the characterized asperity model

North fault		Asperity	Background
Seismic moment	(dyne-cm)	1.43×10^{27}	0.61×10^{27}
Effective stress	(bar)	27.3	5.5
South fault		Asperity	Background
Seismic moment	(dyne-cm)	0.95×10^{27}	0.41×10^{27}
Effective stress	(bar)	29.8	5.5

SIMULATION AT JMA SAPPORO BY EMPIRICAL GREEN'S FUNCTION METHOD**Fault parameters of aftershocks as empirical Green's functions**

We chose two aftershocks as empirical Green's functions, the aftershock 1 of July 13, 1993, and the aftershock 2 of August 8, 1993. We used the focal mechanisms of the mainshock, the aftershock 1, and the aftershock 2 derived by Harvard University [14], Imanishi *et al.* [11], and Iwata *et al.* [16], respectively, shown in Figure 1. The mainshock and two aftershocks have almost the same focal mechanism. In this paper, the aftershock 1 is used as the empirical Green's function for the north fault, and the aftershock 2 is used as the empirical Green's function for the south fault.

The fault length L , the fault width W , the final slip D , and the effective stress σ are needed for the empirical Green's function method by Dan and Sato [9]. These four parameters are related by

$$M_0 = \mu LWD, \quad (22)$$

$$\sigma = (7\pi/16)(\mu D/\lambda), \quad \lambda = \sqrt{LW/\pi}. \quad (23)$$

Here, M_0 is listed in Table 3, λ is the equivalent radius of the fault, and σ is assumed to equal to the stress drop $\Delta\sigma$ [6]. The circular corner frequency ω_c is described in the ω^{-2} model proposed by Brune [17] as follows:

$$\omega_c = 2\beta\sqrt{\pi\lambda\sigma/M_0}. \quad (24)$$

Because the circular corner frequency ω_c is determined from the acceleration record at JMA Sapporo, the fault parameters of the aftershocks 1 and 2 are calculated as listed in Table 4.

Table 4 The source parameters of the aftershocks for empirical Green's functions

		Aftershock 1	Aftershock 2
Date		13 July 1993	8 August 1993
Epicenter		42° 43' 18" N 139° 20' 00" E	41° 57' 18" N 139° 53' 06" E
Focal depth	(km)	28.8	23.7
Magnitude	M_{JMA}	6.0	6.3
Seismic moment	(dyne-cm)	1.1×10^{25}	1.76×10^{25}
Short-period level	(dyne-cm/s ²)	1.92×10^{25}	3.36×10^{25}
Strike		N162E	N347E
Dip		42W	53E
Rake		83	64
Fault length	(km)	13.5	12.9
Fault width	(km)	13.5	12.9
Final slip	(m)	0.102	0.179
Effective stress	(bar)	10.8	19.8
Corner frequency	(Hz)	0.21	0.22
Density	(g/cm ³)	3.2	3.2
S-wave velocity	(km/s)	4.3	4.3

Simulation results at JMA Sapporo

The synthesis procedure was applied to the variable-slip rupture model of the Hokkaido-Nansei-Oki earthquake to simulate the acceleration records at JMA Sapporo. Here, the hypocenter is near the center of the north fault ($42^{\circ} 47' 06''$ N, $139^{\circ} 13' 55''$ E, depth=20km), and the rupture is assumed to propagate radially with velocity of 3.0 km/s. The rupture of the south fault is assumed to start 17 seconds after the rupture of the north fault, the initiation point of the south fault is assumed to be the north-east corner of the fault ($42^{\circ} 31' 25''$ N, $139^{\circ} 15' 17''$ E, depth=2km), and the velocity of the rupture propagation and the rupture mode are assumed to be the same as those of the north fault. The quality factor, Q , is assumed to be a constant value of 500, and does not depend on frequency.

Figure 5 shows the acceleration waveforms of the simulation results by the variable-slip rupture model, the asperity model A, and the asperity model B, and the acceleration record of the mainshock. All the accelerations are the N-S components. Figure 6 shows the integrated motions. All the results in Figures 5 and 6 are filtered by a band-pass filter in the period range of 0.1 to 20 seconds. The simulated mainshock motions are in good agreement with the observed ones for the peak acceleration, the peak velocity, and the envelope characteristics.

Figure 7 shows the pseudo-velocity response spectra with a damping factor of 5% for N-S component by the observed motion and the simulated motions. The spectra by the simulated motions are in good agreement with that by the observed motion except at periods around 3 and 10 seconds. The asperity model A, whose asperity was arranged at the shallow position according to the final slip distribution of the variable-slip rupture model, reproduced the long-period earthquake motion of about 10 seconds, but this model produced a slightly larger short-period earthquake motion in the period range of 0.5 to 1.5 seconds than the records. The asperity model B, whose asperity was arranged at the deep position according to the seismic moment or the short-period level distribution of the variable-slip rupture model, reproduced the short-period earthquake motion of the record in the period range of 0.5 to 1.5 seconds, but this model produced a smaller long-period earthquake motion at around 10 seconds than the records.

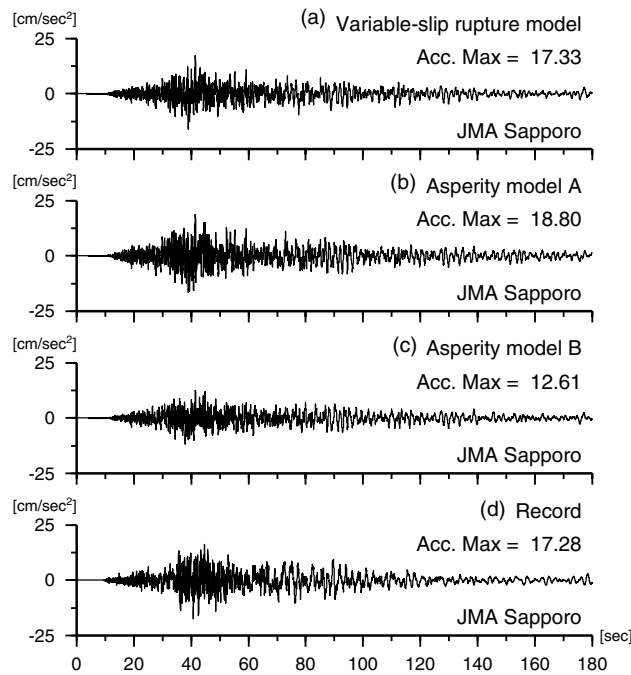


Figure 5 Acceleration waveforms at JMA Sapporo for the mainshock (N-S component)

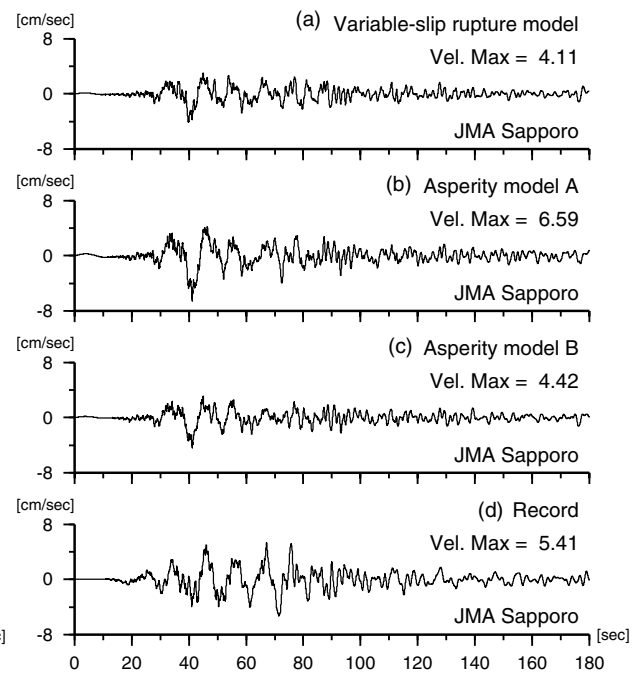


Figure 6 Velocity waveforms at JMA Sapporo for the mainshock (N-S component)

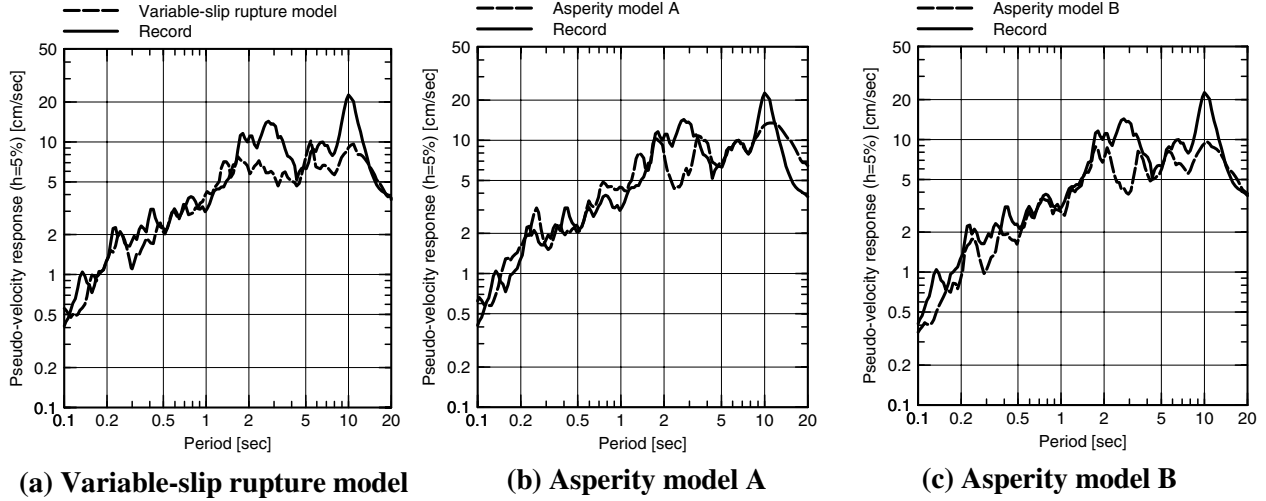


Figure 7 Pseudo-velocity response spectra with a damping factor of 5% at JMA Sapporo for the mainshock (N-S component)

SIMULATION AT JMA SAPPORO BY STOCHASTIC GREEN'S FUNCTION METHOD

Outline to generate stochastic Green's functions

We generated the stochastic Green's functions on the engineering bedrock by the method of Dan *et al.* [18].

First, the acceleration Fourier spectrum $A_{iq}(f)$ of the stochastic Green's functions for the principal part of S-wave on the engineering bedrock is described by

$$A_{iq}(f) = \frac{F}{4\pi\rho_{iq}\beta_{iq}^3} \frac{M_{0iq}(2\pi f)^2}{1+(f/f_{ciq})^2} \frac{1}{\sqrt{1+(f/f_{maxiq})^m}} \times \frac{1}{r_{iq}} \exp\left[-\frac{\pi f r_{iq}}{Q(f)\beta_{iq}}\right] \times 2\sqrt{\frac{\rho_{iq}\beta_{iq}}{\rho_{eb}\beta_{eb}}}, \quad (25)$$

where i means the north or south fault, q is numbered in the depth from shallow position to deep position, F is the radiation pattern, ρ_{iq} and β_{iq} are the density and the shear wave velocity of the subfault, M_{0iq} is the seismic moment, f_{ciq} is the corner frequency, f_{maxiq} is the cut off frequency, m is constant for f_{maxiq} , r_{iq} is a distance from the site to the center of the subfault, $Q(f)$ is the quality factor of the crust, and ρ_{eb} and β_{eb} are the density and the shear wave velocity of the engineering bedrock. The last term of equation (25) is for the free field effect and for the difference of impedance of the source and the engineering bedrock.

Next, the phase characteristics are given by the envelope characteristics derived from the principal part of the S-waves on the engineering bedrock in Sendai area [19].

Verification of the stochastic Green's function by the records at JMA Sapporo during the aftershock 1

We generated the stochastic Green's function at JMA Sapporo by using the source parameter of the aftershock 1 (M_{JMA} 6.0), and compared it with the observed records to verify the stochastic Green's function. The source parameters of the aftershock 1 are listed in Table 4.

For other parameters in the equation (25), ρ_{eb} is 1.8 g/cm³ referring to the bedrock data at Sapporo (HDK180) of Kyoshin Net (K-NET) by the National Information Center for Earthquakes and Disasters, Japan, β_{eb} is assumed 450 m/s, $Q(f)$ is 500 taken from Mendoza and Fukuyama [13], F is 0.62 which is average of the radiation pattern of the SV-wave by Boore and Boatwright [20], and f_{max} is 13.5 Hz and m is 4.2 taken from Sato *et al.* [21].

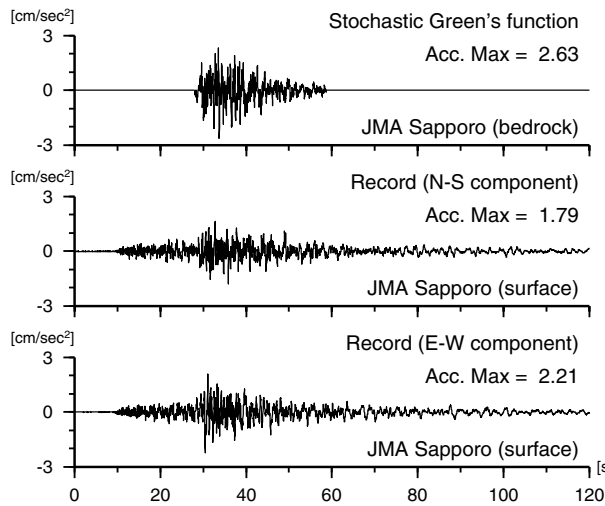


Figure 8 Acceleration waveforms of the stochastic Green's function and the records at JMA Sapporo for the aftershock 1

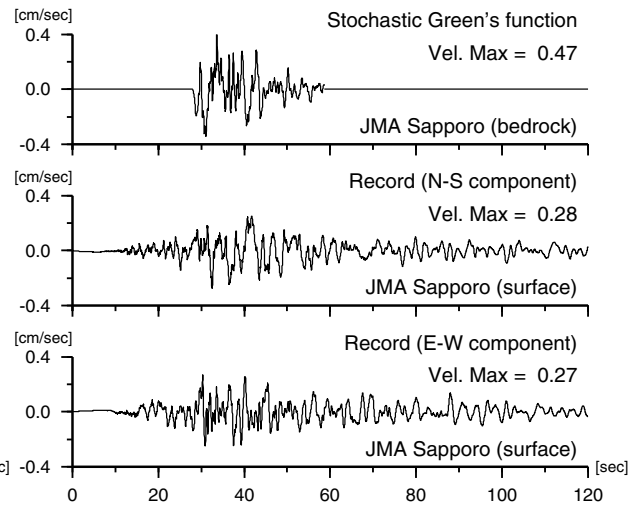


Figure 9 Velocity waveforms of the stochastic Green's function and the records at JMA Sapporo for the aftershock 1

Figures 8 and 9 show the acceleration and the velocity waveforms of the stochastic Green's function, respectively, with the observed records on the surface. The stochastic Green's function and the observed records are filtered by a band-pass filter in the period range of 0.1 to 20 seconds. The principal motion of the S-waves is simulated well, while the P-waves or the coda waves are not simulated because the stochastic Green's function method adopted in this study can be applied to the principal motion of the S-waves only.

On the other hand, the response spectrum on the surface was calculated by multiplying response spectra with a damping factor of 5% of the stochastic Green's function on the engineering bedrock and the amplification factor from the engineering bedrock to the surface in the period range of 0.1 to 4 seconds at JMA Sapporo [22]. Figure 10 shows the pseudo-velocity response spectra with a damping factor of 5% by the simulated motions on the surface with the observed records for the aftershock 1. The response spectrum by the simulated motions and those by the records are in good agreement except the long-period range about more than 2 seconds.

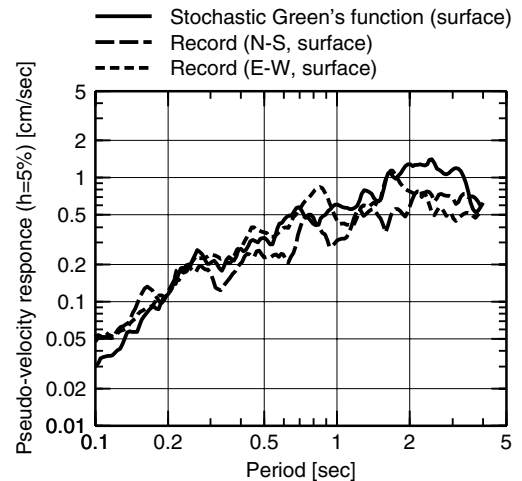


Figure 10 Pseudo-velocity response spectra with a damping factor of 5% of the stochastic Green's function and the records at JMA Sapporo for the aftershock 1

Generation of the stochastic Green's functions for the simulation at JMA Sapporo for the mainshock

We generated a total of 14 stochastic Green's functions on the engineering bedrock at JMA Sapporo for the mainshock, 7 for the north fault and 7 for the south fault. The hypocenters of the stochastic Green's function are placed at the

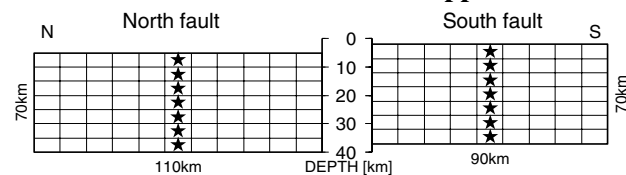


Figure 11 The hypocenters for the stochastic Green's functions for the mainshock simulation

center of each depth at the north fault and the south fault as shown in Figure 11. The parameters ρ_{iq} and β_{iq} vary with the depth of the subfault, and the fault length L_{iq} and the fault width W_{iq} is 10 km and 10 km, respectively. The final slip D is 0.1 m, and the seismic moment M_{0iq} and the corner frequency f_{ciq} are calculated by the equations (22) to (24). Magnitude of JMA was converted from the seismic moment [23]. All parameters for the calculation are listed on the Table 6.

Table 6 The parameters for generating the stochastic Green's functions

(a) Common parameters of the north fault and the south fault

Fault length	L	(km)	10
Fault width	W	(km)	10
Final slip	D	(m)	0.1
Radiation pattern	F		0.62
f_{\max}	$f_{\max iq}$	(Hz)	13.5
Constant for f_{\max}	m		4.2
Q	Q		500
Density (bedrock)	ρ_{eb}	(g/cm ³)	1.8
S-wave velocity (bedrock)	β_{eb}	(m/s)	450

(b) Parameters of the north fault

Layer No.	Depth	Density	S-wave velocity	Rigidity	Seismic moment	Magnitude	Effective stress	Corner frequency
q	(km)	ρ_{iq} (g/cm ³)	β_{iq} (km/s)	μ_{iq} (dyne/cm ²)	M_{0iq} (dyne-cm)	M_{JMAiq}	σ_{iq} (bar)	f_{ciq} (Hz)
1	5 – 10	2.7	3.3	2.9×10^{11}	2.9×10^{24}	5.5	7.2	0.22
2	10 – 15	2.8	3.6	3.6×10^{11}	3.6×10^{24}	5.6	8.8	0.24
3	15 – 20	2.9	3.8	4.2×10^{11}	4.2×10^{24}	5.6	10.2	0.25
4	20 – 25	3.2	4.3	5.9×10^{11}	5.9×10^{24}	5.7	14.4	0.28
5	25 – 30	3.2	4.3	5.9×10^{11}	5.9×10^{24}	5.7	14.4	0.28
6	30 – 35	3.2	4.3	5.9×10^{11}	5.9×10^{24}	5.7	14.4	0.28
7	35 – 40	3.2	4.3	5.9×10^{11}	5.9×10^{24}	5.7	14.4	0.28

(c) Parameters of the south fault

Layer No.	Depth	Density	S-wave velocity	Rigidity	Seismic moment	Magnitude	Effective Stress	Corner frequency
q	(km)	ρ_{iq} (g/cm ³)	β_{iq} (km/s)	μ_{iq} (dyne/cm ²)	M_{0iq} (dyne-cm)	M_{JMAiq}	σ_{iq} (bar)	f_{ciq} (Hz)
1	2 – 7	2.3	2.0	9.2×10^{10}	9.2×10^{23}	5.2	2.2	0.13
2	7 – 12	2.7	3.3	2.9×10^{11}	2.9×10^{24}	5.5	7.2	0.22
3	12 – 17	2.9	3.8	4.2×10^{11}	4.2×10^{24}	5.6	10.2	0.25
4	17 – 22	3.0	4.0	4.8×10^{11}	4.8×10^{24}	5.7	11.7	0.26
5	22 – 27	3.2	4.3	5.9×10^{11}	5.9×10^{24}	5.7	14.4	0.28
6	27 – 32	3.2	4.3	5.9×10^{11}	5.9×10^{24}	5.7	14.4	0.28
7	32 – 37	3.2	4.3	5.9×10^{11}	5.9×10^{24}	5.7	14.4	0.28

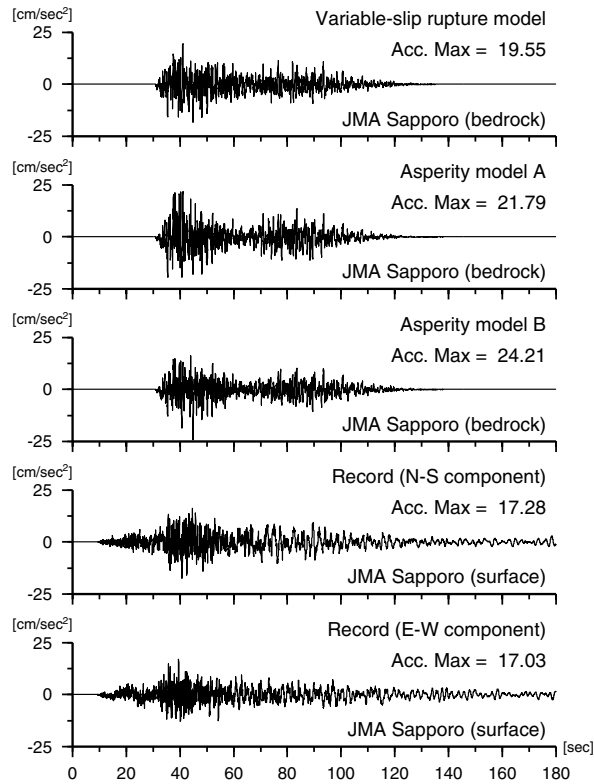


Figure 12 Acceleration waveforms of the simulated motions on bedrock and the records on the surface at JMA Sapporo for the mainshock

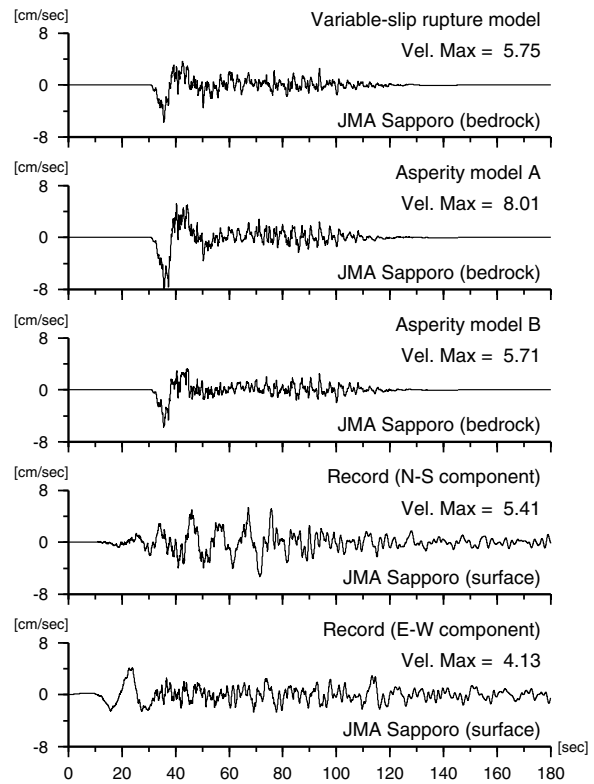


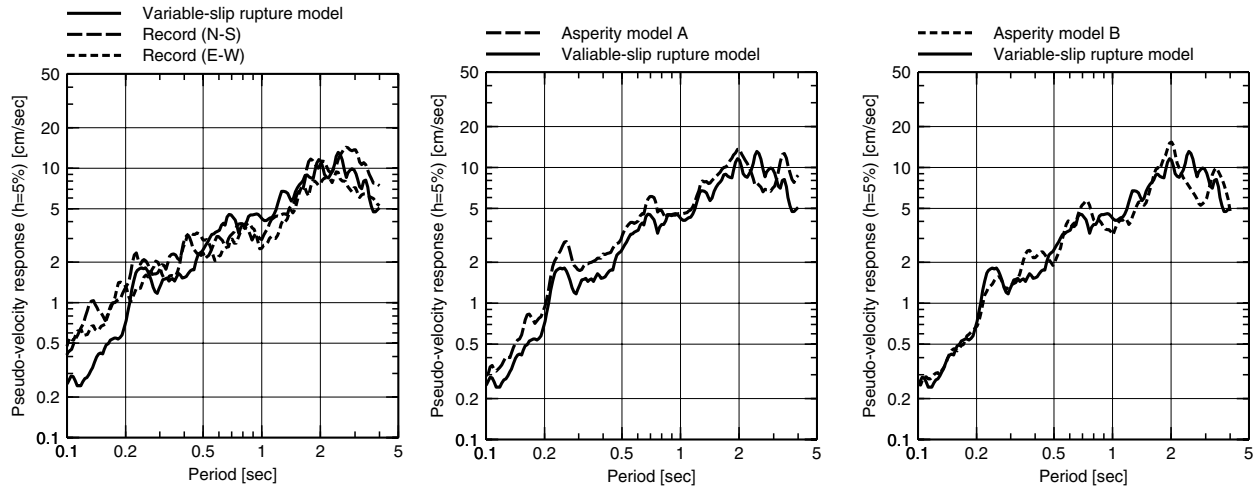
Figure 13 Velocity waveforms of the simulated motions on bedrock and the records on the surface at JMA Sapporo for the mainshock

Simulation results at JMA Sapporo for the mainshock

The stochastic Green's function method was applied to the simulation at JMA Sapporo with the variable-slip rupture model and the two characterized asperity models A and B. The 14 stochastic Green's functions were used.

Figure 12 shows the simulated motions at JMA Sapporo for the variable-slip rupture model, the asperity model A, and the asperity model B, and the observed motions of N-S and E-W components. All the motions are filtered by a band-pass filter in the period range of 0.1 to 20 seconds. Figure 13 shows the velocity waveforms according to the acceleration waveforms in Figure 12. The simulated motions and the observed records can't be compared directly, because the former is on the engineering bedrock and the latter is on the surface. The simulated motions do not include the P-waves, especially the large and long-period pulse in the velocity wave of E-W component, or the coda waves.

The response spectrum on the surface was calculated by multiplying response spectra with a damping factor of 5% on the engineering bedrock and the amplification factor from the engineering bedrock to the surface in the period range of 0.1 to 4 seconds at JMA Sapporo [22]. Figure 14a shows the pseudo-velocity response spectrum with a damping factor of 5% by the variable-slip rupture model on the surface with those of the observed records of the mainshock. These spectra are in pretty good agreement in the period range longer than 0.2 seconds. Figures 14b and 14c show the pseudo-velocity response spectra with a damping factor of 5% by the asperity models A and B on the surface with that by the variable-slip rupture model. From the results, the pseudo-velocity response spectrum by the asperity model B is in good agreement with that by the variable-slip rupture model in the wide period range, and the pseudo-velocity response spectrum by the asperity model A is slightly larger than that by the variable-slip rupture model in the period range of 0.1 to 0.5 seconds.



(a) Variable-slip rupture model and records (b) Variable-slip rupture model and asperity model A (c) Variable-slip rupture model and asperity model B

Figure 14 Pseudo-velocity response spectra with a damping factor of 5% on the surface at JMA Sapporo for the mainshock

SIMULATION IN THE WIDE AREA FOR THE MAINSHOCK BY STOCHASTIC GREEN'S FUNCTION METHOD

We simulated strong ground motions in the wide area (from 39° N to 44° N, from 138° E to 142° E, 600 km x 320 km=192,000 km²) during the 1993 Hokkaido-Nansei-Oki earthquake based on its variable-slip rupture model and on its characterized asperity models A and B by the stochastic Green's function method. Figure 15 shows the calculation flow. First, we simulated the acceleration wave on the engineering bedrock whose shear wave velocity was 450 m/s in every 1 km², and integrated the acceleration wave to the velocity wave to calculate the peak velocity. Next, we calculated the amplification factor from the engineering bedrock to the surface by Matsuoka and Midorikawa [24], and calculated the peak velocities on the surface. Then, we calculated the distribution of the instrumental seismic intensities on the surface by converting the peak velocities using the empirical relation of Tong and Yamazaki [25].

Figure 16 shows the distribution of the peak velocity on the engineering bedrock by the variable-slip rupture model. From the result, the peak velocity is large on the north fault around the hypocenter and the upper side on the south fault, and the distribution of the peak velocity is decreasing in the shape of an ellipse.

Figure 17 shows the distribution of the instrumental seismic intensities on the surface by the variable-slip rupture model. The instrumental seismic intensities are large at Okushiri Island near the hypocenter and the western coast of Hokkaido, and they get smaller as they get further from the fault.

Figure 18 compares the instrumental seismic intensity by the variable-slip rupture model and by the characterized asperity models A and B with that by the questionnaire [26]. The instrumental seismic intensity by the variable-slip rupture model reproduces the questionnaire seismic intensity. Both two asperity models also reproduce the questionnaire seismic intensity. However the asperity model B reproduces the instrumental seismic intensity by the variable-slip rupture model better than the asperity model A.

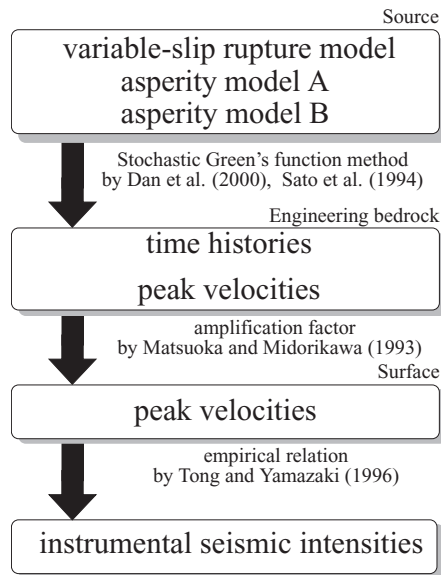


Figure 15 Calculation flow of the instrumental seismic intensities

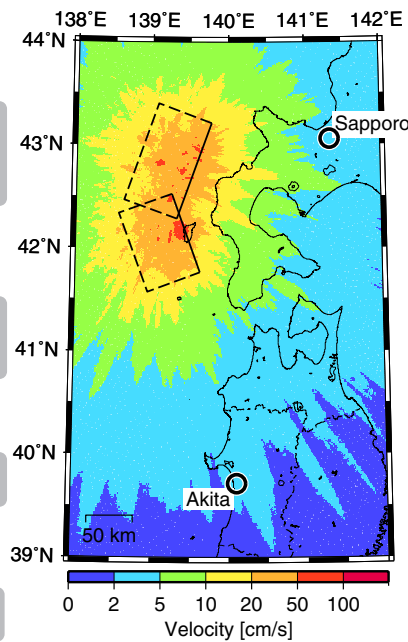


Figure 16 Distribution of the peak velocity on the engineering bedrock by the variable-slip rupture model

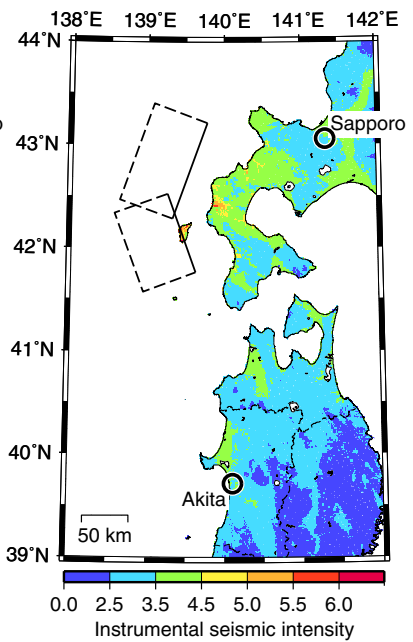
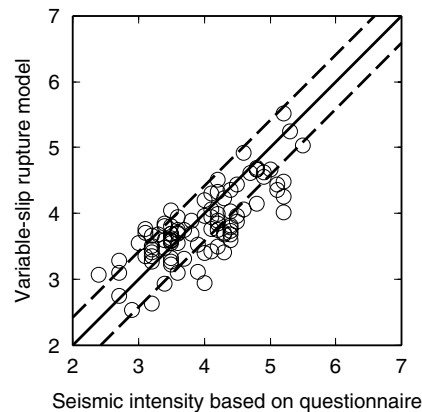
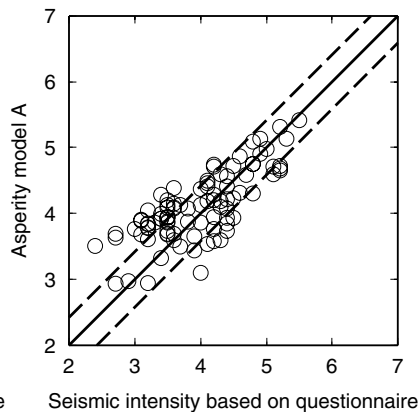


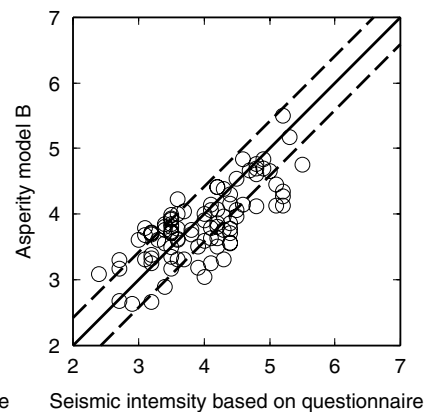
Figure 17 Distribution of the instrumental seismic intensity on the surface by the variable-slip rupture model



(a) Variable-slip rupture model



(b) Asperity model A



(c) Asperity model B

Figure 18 Comparison between the instrumental seismic intensity base on the questionnaire and those based on the simulated motions

CONCLUSIONS

We simulated strong ground motions during the 1993 Hokkaido-Nansei-Oki, Japan, earthquake (M_{JMA} 7.8) based on its variable-slip rupture model and on its characterized asperity models to verify the characterizing procedure of the sources for the strong motion prediction in future earthquakes. The sources were characterized by the total seismic moment, the short-period level of the source spectra, and

the ratios of the area, the final slip, and the effective stress on the asperity to those on the entire fault (Dan *et al.* [1]).

First, the empirical Green's function method proposed by Dan and Sato [9] was applied to the simulation of the records at JMA Sapporo, about 170 km far from the fault, and the following results were obtained:

1) The asperity model, whose asperity was arranged at the shallow position according to the final slip distribution of the variable-slip rupture model, reproduced the long-period earthquake motion of 10 seconds, but this model produced a slightly larger short-period earthquake motion of 0.5 to 1.5 seconds than the records.

2) The asperity model, whose asperity was arranged at the deep position according to the seismic moment or short-period level distribution of the variable-slip rupture model, reproduced the short-period earthquake motion of 0.5 to 1.5 seconds, but this model produced a less long-period earthquake motion of 10 seconds than the records.

Next, the stochastic Green's function method proposed by Dan *et al.* [18] was applied to the wide area (192,000 km²) including the epicentral region, and the following results were obtained:

1) The asperity model, whose asperity was arranged at the shallow position according to the final slip distribution of the variable-slip rupture model, produced a slightly larger seismic intensity than the variable-slip rupture model did.

2) On the other hand, the asperity model, whose asperity was arranged at the deep position according to the short-period level distribution of the variable-slip rupture model, produced the same seismic intensity as the variable-slip rupture model did.

REFERENCES

1. Dan K, Watanabe M, Sato T and Ishii T. "Short-period source spectra inferred from variable-slip rupture models and modeling of earthquake faults for strong motion prediction by semi-empirical method", Journal of Structural and Construction Engineering, Architectural Institute of Japan, 2001; No.545: 51-62. (in Japanese)
2. Heaton TH, Hall JF, Wald DJ and Halling MW. "Response of high-rise and base-isolated buildings to a hypothetical M_w 7.0 blind thrust earthquake", Science, 1995; Vol.267: 206-211.
3. Kikuchi M and Fukao Y. "Inversion of long-period P-waves from great earthquakes along subduction zones", Tectonophysics, 1987; Vol.144, Nos. 1-3: 231-247.
4. Somerville P, Irikura K, Graves R, Sawada S, Wald D, Abrahamson N, Iwasaki Y, Kagawa T, Smith N and Kowada A. "Characterizing crustal earthquake slip models for the prediction of strong ground motion", Seismological Research Letters, 1999; Vol.70, No.1: 59-80.
5. Irikura K and Miyake H. "Procedure of characterized-source modeling for strong ground motion prediction", Abstracts of the Seismological Society of Japan, fall meeting, 2000; P104. (in Japanese)
6. Eshelby JD. "The determination of the elastic field of an ellipsoidal inclusion, and related problems", Proceedings of the Royal Society of London, 1957; Series A, Vol.241: 376-396.
7. Kamae K and Irikura K. "A source model of the 1994 Northridge earthquake ($M_w=6.7$)", Proceedings of the 10th Earthquake Engineering Symposium, 1998; Vol.1: 643-648. (in Japanese)
8. Kamae K and Irikura K. "A fault model of the 1995 Hyogo-ken Nanbu Earthquake and simulation of strong ground motion in near-source area", Journal of Structural and Construction Engineering, Architectural Institute of Japan, 1997; No.500: 29-36. (in Japanese)
9. Dan K and Sato T. "Strong-motion prediction by semi-empirical method based on variable-slip rupture model of earthquake fault", Journal of Structural and Construction Engineering, Architectural Institute of Japan, 1998; No.509: 49-60. (in Japanese)

10. Kikuchi M. "Source process of the Hokkaido Nansei-Oki earthquake of July 12, 1993 inferred from teleseismic body wave inversion", Abstracts of the Seismological Society of Japan, fall meeting, 1993; No.2: 28. (in Japanese)
11. Imanishi K, Ikeda I and Sato T. "A rupture process of the 1993 Hokkaido-Nansei-Oki earthquake derived from the empirical Green function method", Zisin, Journal of the Seismological Society of Japan, 1995; Vol.2, 48(3): 365-373. (in Japanese)
12. Kakehi Y and Irikura K. "High-Frequency radiation process during earthquake faulting – Envelop inversion of acceleration seismograms from the 1993 Hokkaido-Nansei-Oki, Japan, earthquake", Bulletin of the Seismological Society of America, 1997; Vol.87, No.4: 904-917.
13. Mendoza C and Fukuyama E. "The July 12, 1993, Hokkaido-Nansei-Oki, Japan, earthquake: Coseismic slip pattern from strong-motion", Journal of Geophysical Research, 1996; Vol.101, No.B1: 791-801.
14. Harvard University, <http://www.seismology.harvard.edu/CMTsearch.html>.
15. Ishii T, Sato T and Somerville P. "Identification of main rupture areas of heterogeneous fault models for strong-motion estimation", Journal of Structural and Construction Engineering, Architectural Institute of Japan, 2000; No.527: 61-70. (in Japanese)
16. Iwata T, Irikura K and Kamae K., KAIYO MONTHLY, 1994; No.7: 80-87. (in Japanese)
17. Brune JN. "Tectonic stress and the spectra of seismic shear waves from earthquakes", Journal of Geophysical Research, 1970; Vol.75, No.26: 4997-5009.
18. Dan K, Watanabe M, Sato T, Miyakoshi J and Sato T. "Isoseismal map of strong motions for the 1923 Kanto earthquake (M_{JMA} 7.9) by stochastic Green's function method", Journal of Structural and Construction Engineering, Architectural Institute of Japan, 2000; No.530: 53-62. (in Japanese)
19. Sato T, Kawase H and Sato T. "Engineering bedrock waves obtained through the identification analysis based on borehole records and their statistical envelope characteristics", Journal of Structural and Construction Engineering, Architectural Institute of Japan, 1994; No.461: 19-28. (in Japanese)
20. Boore D and Boatwright J. "Average body-wave radiation coefficients", Bulletin of the Seismological Society of America, 1984; Vol.74, No.5: 1615-1621.
21. Sato T, Kawase H and Sato T. "Statistical spectral characteristics for engineering bedrock waves in which local site effects of surface geology are removed – Based on the ground motion records of small and medium earthquakes observed in the boreholes in Sendai –", Journal of Structural and Construction Engineering, Architectural Institute of Japan, 1994; No.462: 79-89. (in Japanese)
22. Annaka T, Yamazaki F and Katahira F. "A proposal of an attenuation model for peak ground motions and 5% damped acceleration response spectra based on the JMA-87 type strong motion accelerograms", Proceedings of the 24th JSCE Earthquake Engineering Symposium, Earthquake Engineering Committee Japan Society of Civil Engineers, 1997: 161-164. (in Japanese)
23. Sato R. "Parameter handbook of seismic fault in Japan", Kajima publishing, 1989. (in Japanese)
24. Matsuoka M and Midorikawa S. "Prediction of isoseismal map for large area using the digital national land information", Journal of Structural and Construction Engineering, Architectural Institute of Japan, 1993; No.447: 51-56. (in Japanese)
25. Tong H and Yamazaki F. "Relationship between ground motion indices and new JMA seismic intensity", SEISAN-KENKYU Monthly Journal of Institute of Industrial Science, University of Tokyo, 1996; Vol.48, No.11: 31-34. (in Japanese)
26. Takai N, Kagami H and Okada S. "Seismic intensity questionnaire survey on the 1993 Hokkaido-nanseioki earthquake", Architectural Institute of Japan, Summaries of Technical Papers of Annual Meeting, 1994; Structures II: 305-306. (in Japanese)